Earth's Future

RESEARCH ARTICLE
10.1029/2018EF000890

Satellite-Observed Major Greening and Biomass Increase in South China Karst During Recent Decade

Martin Brandt[1], Yuemin Yue[2], Jean Pierre Wigneron[3], Xiaowei Tong[2], Feng Tian[1], Martin Rudbeck Jepsen[1], Xiangming Xiao[4,5], Aleixandre Verger[6,7], Arnaud Mialon[8], Amen Al-Yaari[3], Kelin Wang[2], and Rasmus Fensholt[1]

[1]Department of Geosciences and Natural Resource Management, University of Copenhagen, Copenhagen, Denmark, [2]Key Laboratory for Agro-ecological Processes in Subtropical Region, Institute of Subtropical Agriculture, Chinese Academy of Sciences, Changsha, China, [3]ISPA, INRA, Bordeaux, France, [4]Department of Microbiology and Plant Biology, University of Oklahoma, Norman, OK, USA, [5]Ministry of Education Key Laboratory for Biodiversity Science and Ecological Engineering, and Coastal Ecosystem Research Station of the Yangtze River Estuary, Fudan University, Shanghai, China, [6]CSIC, Global Ecology Unit CREAF-CSIC-UAB, Bellaterra, Spain, [7]CREAF, Cerdanyola del Vallès, Spain, [8]CESBIO, Université de Toulouse, CNES/CNRS/IRD/UPS, Toulouse, France

Key Points:
- We find one of the globally largest increases in vegetation cover and above-ground biomass to occur in South China Karst
- We apply a new Earth observation system based on low frequency passive microwaves to monitor biomass dynamics
- The increase in vegetation cover (69% in 1999; 81% in 2017) occurs over ~1.4 million km^2 and has been generated by widespread conservation efforts

Correspondence to:
Y. Yue,
ymyue@isa.ac.cn

Citation:
Brandt, M., Yue, Y., Wigneron, J. P., Tong, X., Tian, F., Jepsen, M. R., et al. (2018). Satellite-observed major greening and biomass increase in South China karst during recent decade. *Earth's Future*, *6*. https://doi.org/10.1029/2018EF000890

Received 13 APR 2018
Accepted 6 JUN 2018
Accepted article online 15 JUN 2018

Abstract Above-ground vegetation biomass is one of the major carbon sinks and provides both provisioning (e.g., forestry products) and regulating ecosystem services (by sequestering carbon). Continuing deforestation and climate change threaten this natural resource but can effectively be countered by national conservation policies. Here we present time series (1999–2017) derived from complementary satellite systems to describe a phenomenon of global significance: the greening of South China Karst. We find a major increase in growing season vegetation cover from 69% in 1999 to 81% in 2017 occurring over ~1.4 million km^2. Over 1999–2012, we report one of the globally largest increases in biomass to occur in the South China Karst region (on average +4% over 0.9 million km^2), which accounts for ~5% of the global areas characterized with increases in biomass. These increases in southern China's vegetation have occurred despite a decline in rainfall (−8%) and soil moisture (−5%) between 1999 and 2012 and are derived from effects of forestry and conservation activities at an unprecedented spatial scale in human history (~20,000 km^2 yr^{-1} since 2002). These findings have major implications for the provisioning of ecosystem services not only for the Chinese karst ecosystem (e.g., carbon storage, water filtration, and timber production) but also for the study of global carbon cycles.

1. Introduction

The availability of long time series of dense satellite imagery has enabled the scientific community to observe a globally increasing vegetation cover (Fensholt et al., 2012; Nemani et al., 2003; Zhu et al., 2016). This global greening is commonly attributed to an elevated level of atmospheric CO_2 (Piao et al., 2015; Zhu et al., 2016) and changes in the amount and seasonality of rainfall, causing increased plant productivity and encroachment of woody vegetation (Brandt et al., 2017). Several studies have assessed the direct impact of forestry and conservation projects on vegetation (Cao et al., 2014, 2016; Cao & Zhang, 2015; Fang et al., 2014; Tong et al., 2017, 2018; Xiao, 2014; Y. Zhang et al., 2016), yet the significance of such projects on global biomass and vegetation cover trends is rarely studied.

The South China Karst region is one of the largest exposed carbonate rock areas in the world, covering ~1.9 million km^2 (~0.54 million km^2 underlain by carbonate rocks) and hosting more than 200 million people in eight provinces (Zhang et al., 2017). Accelerating land degradation has been reported as a result of increased exploitation of natural resources during the last half century (Jiang et al., 2014). Population pressure led farmers to increasingly expand to sloping areas and as a result, large parts of the karst area were deforested, exposing the soil to erosion. Consequently, a significant area of karst (~0.13 million km^2) previously covered by shrubs and trees was gradually converted to bare soils. The loss of soil and vegetation cover was detrimental from both an ecological and economical point of view: The karst aquifer is an important water reservoir, but the reduction in vegetation cover resulted in surface runoff and decreased infiltration rates. Moreover, local livelihoods depending on agriculture lost their source of income resulting in aggravated rate of poverty, which is estimated to affect 50 million people (Jiang et al., 2014; J. Zhang et al., 2016).

To combat this case of land degradation and to alleviate poverty, the Chinese government has invested more than US$19 billion in mitigation initiatives since the turn of the new millennium. Considering this investment and the spatial extent, China's ecological engineering projects are known as the most ambitious afforestation and conservation projects in human history (Moore et al., 2016). These projects are aimed at converting farmlands and degraded lands into conservation or production forests and grasslands (Delang & Yuan, 2015). Farmers are provided with tree saplings and a compensation payment if trees are planted on sloped farmlands. The trees provide ecosystem services, and the wood and nontimber products can be sold. In this way, tree plantations have effectively been implemented and most farmlands on sloped hills have been abandoned and are currently covered by shrubs, tree plantations, or secondary and man-made forests (Hua et al., 2016; Ouyang et al., 2016). Furthermore, strict protection laws limit the general use of woody resources, leading to a natural regeneration of the region. Almost two decades after the initiation of project implementations, the humid climate and the selection of robust and fast growing tree species (e.g. *Eucalyptus* spec. and *Zenia insignis*) have led to a significantly increased vegetation cover in large parts of the karst ecosystem (Cai et al., 2014; Tong et al., 2017). While the negative aspects of monocultural plantations have been discussed elsewhere (Chen et al., 2015; Cao, 2008, 2011), the increase in above-ground biomass and the associated carbon sequestration may contribute considerably to the national goals of climate mitigation and could have the potential to be of global impact. Several remote sensing-based studies monitoring land degradation and vegetation cover of South China Karst exist and have shown that trends in both leaf area index and carbon stocks have been considerably altered in conservation areas located in the southern parts of the karst region (Tong et al., 2018; Zhang et al., 2017). Yet the scope of these studies remains local and data sources do not include recent advances in the monitoring of vegetation from space (Brandt et al., 2018; Verger et al., 2014).

Vegetation monitoring from traditional optical Earth observation (EO) data sets is generally limited to the green canopy layer with less sensitivity to the biomass volume of the above-ground vegetation (Tian et al., 2016). Moreover, for satellite systems operating in the optical domain, cloud contamination, signal saturation, and climate induced interannual fluctuations in canopy density make it challenging to consistently assess spatial and temporal patterns in above-ground biomass, of which a major proportion is stored in trunks and branches (Latifi et al., 2015). Here we generate and use data sets based on the measurements of passive microwave emission of land surfaces from different satellites. Two main parameters can be retrieved from passive microwave observations: surface soil moisture and vegetation optical depth (VOD; Wigneron et al., 2007, 2017). The most recent system is the Soil Moisture and Ocean Salinity (SMOS) mission, launched at the end of 2009 and provides first observations at L-band (1.4 GHz; Kerr et al., 2016).

The retrieved VOD index is largely insensitive to atmospheric perturbations and closely related to the water content of the entire vegetation layer, including all vegetation elements such as stems, leaves, and additionally branches and trunks in the case of woody vegetation (Guglielmetti et al., 2007; Wigneron et al., 1995). Contrary to the VOD index retrieved at higher frequencies (>5 GHz, hereafter termed X-VOD), the L-band VOD (hereafter termed L-VOD) is not limited to the upper canopy, shows no saturation over densely vegetated areas, and is almost linearly linked to biomass volumes (Brandt et al., 2018; Konings et al., 2017; Rodríguez-Fernández et al., 2018; Vittucci et al., 2016). This makes L-VOD a well suited proxy for monitoring temporal changes in biomass of forest biomes and marks a new era in vegetation monitoring from space (Wigneron et al., 2017). Our study generates both high- and low-frequency VOD data sets along with conventional optical satellite data to monitor the recent greening and the associated above-ground biomass changes in the South China Karst region. The extent of these changes is related to the spatiotemporal patterns observed at the global scale.

2. Materials and Methods

2.1. Satellite Data

Satellite time series are prone to sensor shifts, orbital drifts, atmospheric conditions, and processing algorithms and thus include considerable bias and uncertainty (Tian et al., 2015). We generate and use four different data sets (Table 1) to study changes at global and regional scales: Two are based on optical remote sensing (GEOV2 Fraction of Vegetation Cover [FCover] and Moderate Resolution Imaging Spectroradiometer [MODIS] normalized difference vegetation index [NDVI]) and two based on passive microwave satellite

Table 1
Overview of Contemporary Satellite Data Sets on Vegetation Monitoring Applied in This Study

	Period	Satellite systems	Characteristics	Proxy	Reference
L-VOD (IC v105)	2011–2017 (25 km)	SMOS	Passive microwave emissions at low frequency	Above-ground biomass, more sensitive to trunks and branches (whole vegetation layer), less to leaves	Wigneron et al. (2017)
X-VOD (v2)	1999–2012 (25 km)	SSM/I, WindSat, AMSR-E	Passive microwave emissions at high frequency	Above-ground biomass, sensitive to leaves, trunks and branches of the upper canopy	Liu et al. (2015)
GEOV2 FCover (v2.0.2)	1999–2017 (1 km)	SPOT VGT, PROBA-V	Optical bands (red, NIR, SWIR)	Fraction of ground covered by green vegetation in % (2-dimensional)	Verger et al. (2014)
MODIS NDVI (MOD13C2 06)	2000–2017 (5.6 km)	Terra MODIS	Ratio of two optical bands (red, NIR)	Index for vegetation greenness and cover (2-dimensional)	Tucker (1979)

Note. All data sets are freely available.

observations (L-VOD and X-VOD). FCover (Figures 1a and 1b) and NDVI are widely used to study the greenness of vegetation cover (Tucker, 1979; Verger et al., 2014), and VOD is a recently established proxy for biomass volumes (Liu et al., 2015).

Vegetation optical depth is considered here as proxy for above-ground biomass of living vegetation and forms the basis of this study. Other data sets are used to provide complementary information on vegetation cover and chlorophyll abundance, and we do not aim at a comparison of the different data sets, nor do we expect the data to be free of uncertainty. As in Momen et al. (2017), rainforests are excluded here, because uncertainties related with cloud cover and saturation are associated with the data sets over these types of forests (Fernandez-Moran et al., 2017). Moreover, deserts and water bodies are removed from the analysis, using the MODIS IGBP land cover mask from 2010 (classes 2, 16, and 0).

2.2. X-VOD and SMOS-IC L-VOD

In this study we consider a VOD index estimated at L-band (L-VOD) from the SMOS observations and a VOD index estimated at X-band (X-VOD) from different satellite systems (Table 1). Unlike optical sensors, these systems are almost insensitive to atmospheric and Sun illumination effects and measure the passive microwave emission of above-ground vegetation components (Wigneron et al., 1995). The satellite sensors can thus sense deeper through the vegetation layer than optical data: the lower the frequency, the greater the depth of emission below the canopy.

Soil Moisture and Ocean Salinity IC L-VOD is a unique data set based on low-frequency observations that allows for monitoring of the vegetation water content (in kg m^{-2}) of the entire vegetation layer but is available only since 2011. The sensitivity of L-VOD to the leaf component is low in comparison to its sensitivity to branches and trunks (Guglielmetti et al., 2007). X-VOD is based on high-frequency VOD (Du et al., 2017), sensing both the green and nongreen parts of the vegetation, and is thus also widely used as a proxy for biomass (Liu et al., 2015; Tong et al., 2018). The higher frequency of the X-VOD sensor makes it more sensitive to smaller vegetation components (such as leaves and twigs) than L-VOD, and X-VOD is mainly sensitive to the characteristics of the upper canopy layer when the vegetation is dense, similar to vegetation indices computed in the optical domain (Liu et al., 2015; Tian et al., 2015, 2016). Consequently, although both the L-VOD and X-VOD indices can be used for biomass monitoring, L-VOD can be efficiently used to sense the entire biomass volume even over dense vegetation canopies (Rodríguez-Fernández et al., 2018; Vittucci et al., 2016; Zhang et al., 2011). The daily X-VOD and L-VOD observations are aggregated to annual medians, strongly reducing undesired effects of noise (e.g., radio frequency interferences; RFIs). Effects of RFIs over China are generally strong and a source of noise for SMOS data (Oliva et al., 2012) but mainly affect northern China. They are carefully filtered out in the generated L-VOD data set by using only observations that have a root mean square error between the measured and modeled brightness temperatures lower than 15 K (Fernandez-Moran et al., 2017). Moreover, we use SMOS data from only the descending orbit, which provides more high-quality observations for the study area than the commonly used data from the ascending orbit. This is because the multiangular SMOS antenna is tilted forward by 32°, meaning it is tilted toward the northern pole for ascending orbits (southern pole for descending orbits). Over China, man-made RFIs are mainly located in the northern part of the country. So due to the antenna tilt, RFIs affect the SMOS observations during ascending orbits but to a much lesser extent during descending orbits.

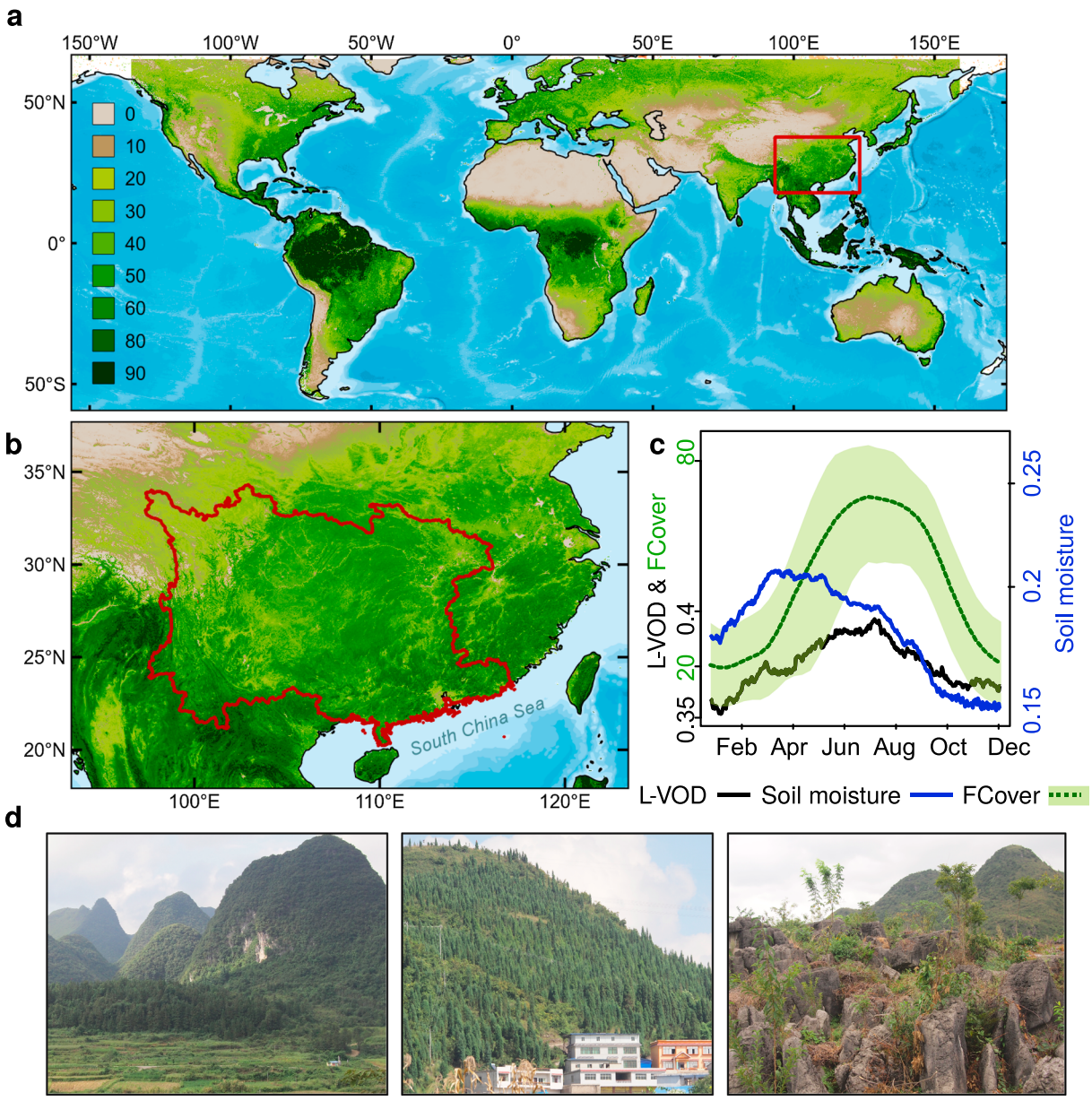

Figure 1. Overview of the study area and major data sets. (a) Global annual mean vegetation cover (GEOV2 FCover 1999–2017). A red rectangle marks Southern China which is zoomed in (b). (b) The study area (red line) is the China karst region spanning eight provinces. (c) Seasonality of FCover (for 2003 in 10-day steps) with 95% confidence interval, SMOS-IC L-VOD, and SMOS-IC soil moisture (averaged 2011–2017 in 1-day steps and shown with a 30-day moving average) for the pixels within the study area. (d) A series of photos taken in October 2017 (1) farmland abandonment and reforestation in the foreground and natural regeneration in the background (2) tree plantings on sloping hills and (3) land degradation.

There exists a good demonstration that X-VOD and L-VOD signal scale with above-ground biomass (Brandt et al., 2018; Liu et al., 2015; Rodríguez-Fernández et al., 2018; Vittucci et al., 2016; Zhang et al., 2011). We thus report relative changes in VOD as proxies of the relative changes in above-ground vegetation biomass at an annual time scale.

2.3. GEOV2 FCover and MODIS NDVI

We apply two additional independent global EO data sets that are not able to assess biomass volumes but are established proxies for the abundance of vegetation (e.g., Myneni & Hall, 1995). GEOV2 FCover and MODIS NDVI are based on independent satellite platforms and cover the full period of conservation efforts in the karst area. FCover corresponds to the fraction of ground covered by green vegetation, that is, the

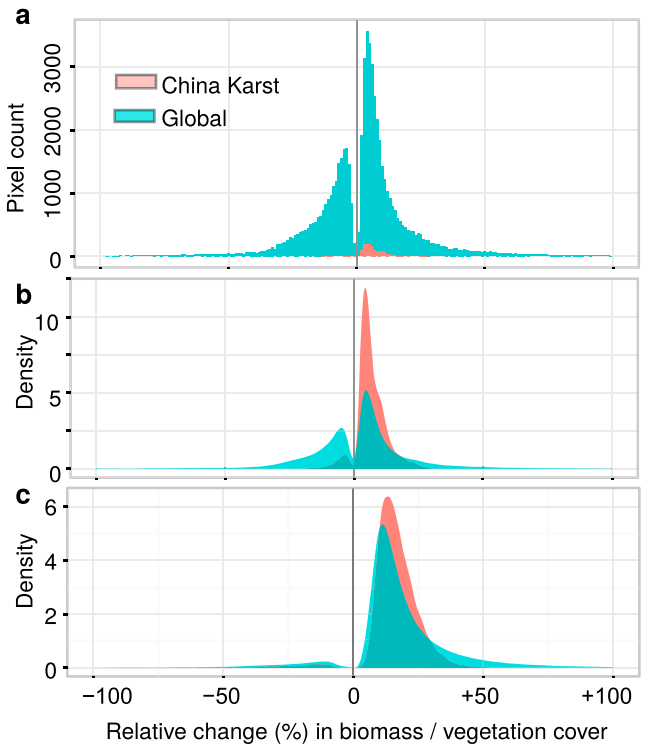

Figure 2. Contribution of China karst (Figure 1b) to significant ($P < 0.05$) global biomass and vegetation cover trends. (a) Histogram of pixels (25×25 km^2) of relative change in X-VOD biomass (1999–2012) for China karst and globally. (b) Same as (a) but as a probability density plot. (c) Probability density plot for vegetation cover (FCover) changes 1999–2017.

vegetation cover (Verger et al., 2014). NDVI is a simple index based on the ratio between red and near infrared bands reflecting the greenness of plants, which is an indirect estimation of vegetation cover (Tucker, 1979). FCover (NDVI) data are delivered cloud-filtered and gap filled in 10 (30)-day steps.

For each pixel and year, we calculate the 90th percentile in the FCover data among the 36 images (12 images for MODIS NDVI), representing the annual growing season conditions. This is preferred over the annual peak value, which may be susceptible to noise. In the following, the value at the 90th percentile in the FCover/NDVI data is termed growing season FCover/NDVI.

2.4. Hydrological and Inventory Data

To study hydrological conditions we use CHIRPS annual rainfall estimates (1999–2017; Funk et al., 2015) as well as soil moisture from the ESA Climate Change Initiative (CCI; 1999–2016) and from the SMOS mission (2011–2017; Kerr et al., 2016). Whereas ESA CCI soil moisture is a combined product of several active and passive microwave satellites (Enenkel et al., 2016), SMOS-IC soil moisture is derived from the same satellite as L-VOD, but the products are independent due to the multiangular and dual-polarization capability of the SMOS system (Wigneron et al., 2017). CCI soil moisture is included because it has a longer temporal availability. Monthly and annually averaged soil moisture estimates serve as a proxy for the root zone soil moisture and are considered as better suited than rainfall as indicators of plant water availability (Momen et al., 2017).

Finally, we include inventory data provided by the State Forestry Administration of China to evaluate annually summed conservation areas and forest plantations (in km^2) in the eight karst provinces (2002–2015; Figures 1a and 1b). The data include the following conservation projects: (1) Natural Forest Protection Project starting in 2001 in 5 provinces, (2) The Grain to Green Programme starting in 2001 in seven provinces with the aim to convert farmland on slopes greater than 25° into ecological and economical forests, (3) Karst Rocky Desertification Comprehensive Control and Restoration Project launched in 2008 in eight provinces with the aim to restore vegetation cover and improve water and soil conservation capabilities, and (4) the River Shelter Forest Project launched in 6 provinces aiming at increasing forest and vegetation cover on the middle and upper reaches of the Yangtze and Zhujiang Rivers to control water and soil erosion. Additionally to conservation activities, extensive tree plantations (e.g. *Eucalyptus* spec, *Pinus massoniana* Lamb, and *Cunninghamia lanceolate*) with economic purposes were established in this area, making the whole region one of the major forestry product producers in China (Chen et al., 2015). It should be noted that the survival rate is around 70% (Delang & Yuan, 2015) and that forest plantations are harvested regularly, making the cumulative number of yearly plantations greatly overestimating the overall plantation area.

2.5. Trend Analysis

We apply a linear regression with the annual satellite time series (annual median for L-VOD and X-VOD and 90th percentile for FCover, NDVI) against time to identify temporal changes and use the *P* value to single out significant trends ($P < 0.05$). To facilitate the comparability of trends between sensors, but also to highlight major changes in areas of less dense vegetation, we report the trends as relative change in percent. This is the per-pixel trend from the start to the end year, that is, the slope (of the linear regression variable against time) multiplied with the number of years and divided by the mean. Anomalies are calculated by the *z*-score (subtract by mean and divide by standard deviation). All analyses are performed in free and open software (GRASS GIS, R, and GDAL).

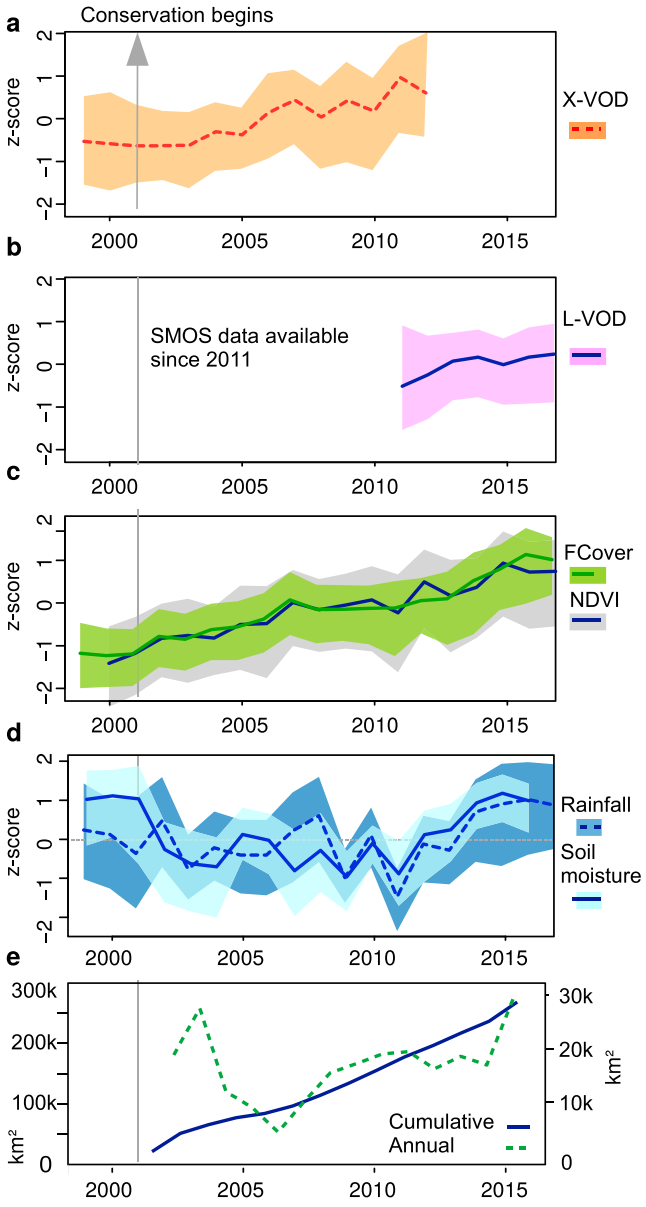

Figure 3. Vegetation and hydrological dynamics 1999–2017 in China karst (Figure 1b). (a) High frequency X-VOD (1999–2012) and (b) low frequency L-VOD (2011–2017). (c) GEOV2 growing season FCover (1999–2017) and MODIS growing season NDVI (2000–2017) together with their 95% confidence intervals (shaded areas). (d) CHIRPS annual rainfall (1999–2017) and CCI soil moisture (1999–2016) with 95% confidence intervals. Annual values are anomalies calculated by the *z*-score. (e) Annual (right y axis) and cumulative (left y axis) extent of forestry and conservation areas in the eight provinces (2002–2015).

2.6. Study Area

The study area is the entire South China Karst region, covering eight provinces (~1.9 million km^2) of which ~0.54 million km^2 can be considered as karst (i.e., is underlain by carbonate rocks; Figures 1a–1d). The natural vegetation is a mixed subtropical evergreen and broadleaf forest, strongly modified or converted by management. Farmers grow mainly rice in river valleys and other lowlands, but population pressure caused farmlands to expand even to steeply sloping hills prior the preproject implementation period. The above-mentioned conservation and restoration programs encourage farmers to abandon farmlands on slopes, and natural regeneration and active plantation projects intended to convert vast areas to shrubland, plantations, and secondary forests (Delang & Yuan, 2015; Jiang et al., 2014). No rainforest/desert/water bodies are present in the study area.

The growing season of vegetation lasts from April to November, with a clear seasonality in vegetation cover ranging from ~20% during boreal winter up to ~80% during the peak time in summer (Figure 1c). The seasonality of L-VOD is low, ranging from ~0.35 to ~0.4, which is caused by the higher sensitivity of L-VOD to persistent vegetation as compared to recurrent vegetation. A lag time in the seasonality between FCover and L-VOD has often been observed over a variety of vegetation types and is caused by the sensitivity of L-VOD to the whole vegetation stratum, while FCover is related to the green canopy layer (Lawrence et al., 2014). Soil moisture is high between March and July but drops to a lower level for the remaining months (Figure 1c).

3. Results

3.1. Global and Regional Changes in Biomass

By using X-VOD (1999–2012) and L-VOD (2011–2017) as a proxy for above-ground biomass, we map percent deviation from the mean for the two periods at a 25 × 25 km spatial resolution. For the 1999–2012 period, there is an overall positive change in biomass at global scale (+2% ±15; $P < 0.05$; Figures 2a and 2b). Areas with a significant ($P < 0.05$) positive biomass trend cover globally ~22 million km^2, of which ~5% are located in the South China Karst region (Figure 2a), making the study area one of the largest, spatially coherent, area of biomass increase (Figures 3a and 4a). More specifically, 55% of the study area show a significant ($P < 0.05$) increase in biomass (on average +4% ±6 over ~0.9 million km^2), of which 0.3 million km^2 are found in karst landscape (representing 64% of the 0.54 million km^2 karst area). This increase occurs in spite of a decrease in rainfall (−8% ±10) over the same period (Figure 3d and Table 2).

After this dry period, positive rainfall anomalies (+38% ±11) favor the L-VOD observed biomass increase which occurs steadily over the studied period (Figures 3b and 3d) from 2011 to 2017 (+11% ±25; Table 2). Note that L-VOD is more stable with less fluctuation than X-VOD (Figures 3a and 3b).

3.2. Global and Regional Changes in Vegetation Cover

We apply GEOV2 FCover and MODIS NDVI to map global changes in vegetation cover from 1999 to 2017. The application of two independent data sets minimizes uncertainty on trends and patterns. These data sets cover the starting phase of forestry and conservation projects (2001) until present and document the karst area as part of a globally increasing vegetation cover over 19 years (Figures 3b, 3c and 4). Overall, the

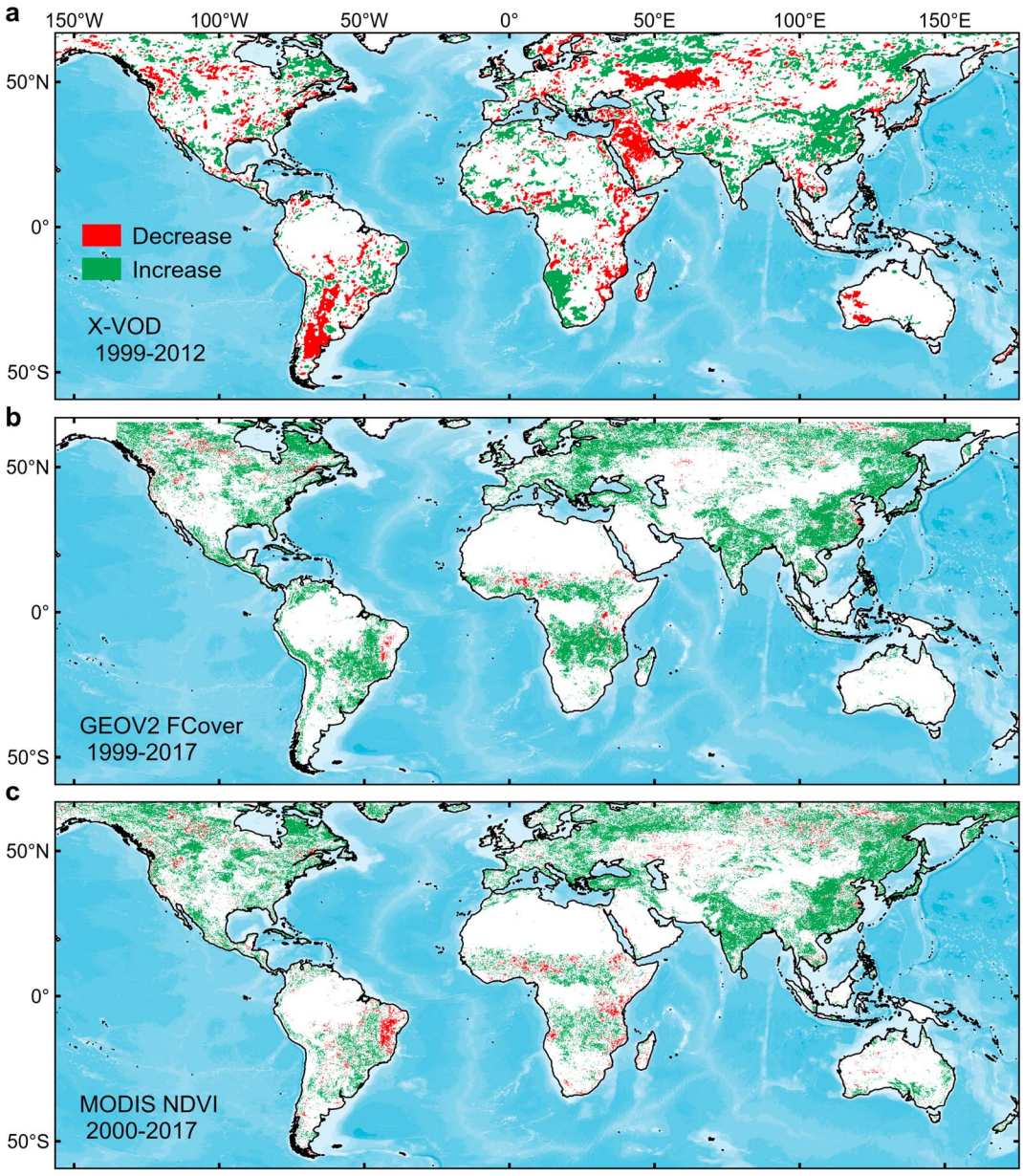

Figure 4. Global maps of significant ($P < 0.05$) increase/decrease. (a) X-VOD annual average 1999–2012, (b) GEOV2 growing season FCover (1999–2017), and (c) MODIS growing season NDVI (2000–2017).

Table 2
Relative Changes in Terms of Trends (%) in the Karst Region (Figure 1b) of the Different Data Sets (Table 1) for Three Periods

	1999–2012	2011–2017	1999–2017
Biomass (SMOS-IC L-VOD)	NA	+11% (0.32–0.35)	NA
Canopy biomass (X-VOD)	+4% (0.78–0.80)	NA	NA
Vegetation cover (GEOV2 FCover)	+7% (69–76%)	+7% (74–81%)	+12% (69–81%)
Greenness (MODIS NDVI) starting 2000	+6% (0.73–0.76)	+4% (0.76–0.79)	+8% (0.73–0.79)
Rainfall (CHIRPS)	−8% (1,341–1,298 mm)	+38% (1,034–1,475 mm)	+10% (1,341–1,475 mm)
Soil moisture (CCI) ending 2016	−5% (0.32–0.31 m^3 m^{-3})	+8% (0.29–0.32 m^3 m^{-3})	+1% (0.32–0.32 m^3 m^{-3})

Note. The numbers in brackets show the rounded start and end values in the corresponding unit for the corresponding period (e.g., FCover was 69% in 1999, 74% in 2011, and 81% in 2017). The start and end values do not always correspond with the trend (% change). No significance test is applied here.

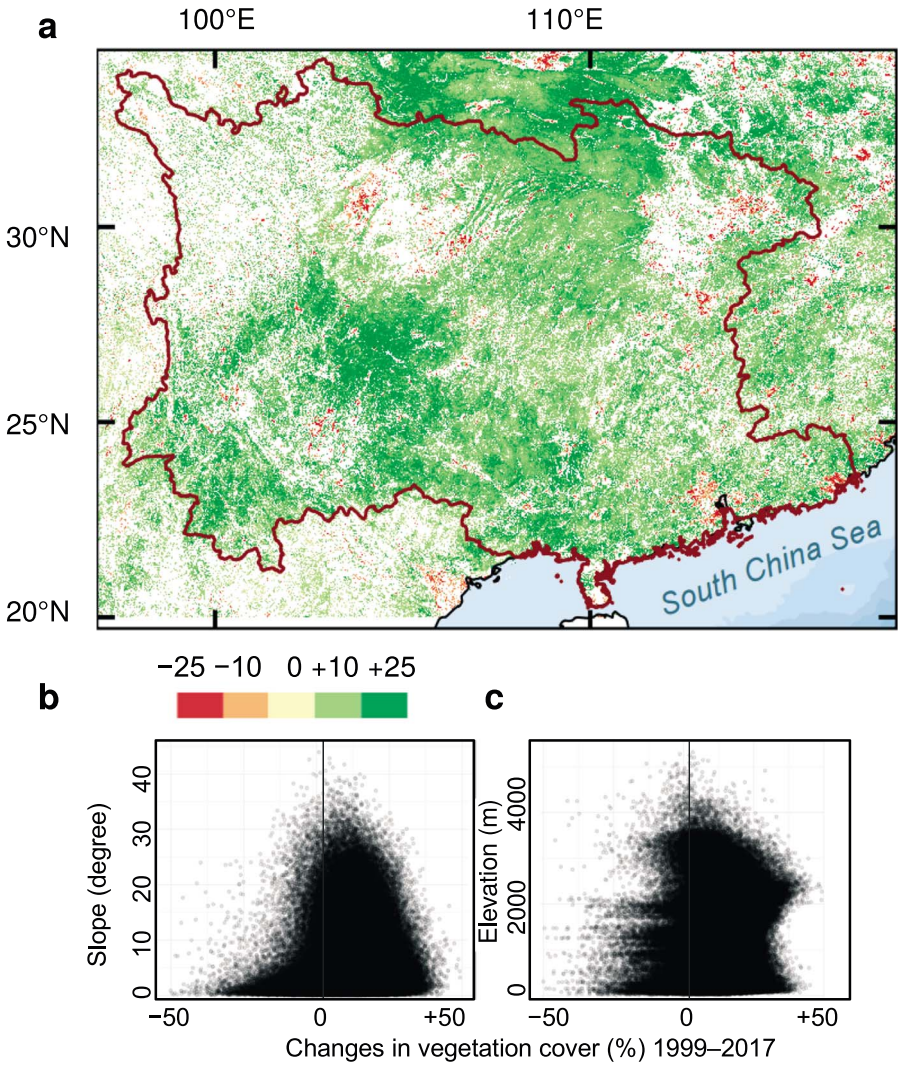

Figure 5. Vegetation cover (FCover) trends in China's karst region. (a) Changes in vegetation cover between 1999 and 2017 in % fractional cover at 1 × 1 km spatial resolution. (b) The relationship between terrain slope (in degree) and changes in vegetation cover. (c) Same as (b) for terrain elevation in meters above sea level.

global change in the vegetation cover (FCover) is positive from 1999 to 2017 (+14% ±28; $P < 0.05$; Figure 2c) on ~40 million km^2, of which 1.4 million km^2 (~4%) are located in the karst region of Southern China (Figures 4b and 4c and 5a). The pattern was confirmed by MODIS NDVI, which is available from 2000 to 2017 (Figure 4c and Table 2).

Following the start of the conservation and afforestation programs in 2001, the vegetation cover rapidly increases (+7%) over the karst region in spite of a decreasing trend in annual rainfall (−8%) and soil moisture (−5%; 1999–2012; Figures 3c and 3d). The increase in vegetation cover levels off around 2007, and further, vegetation growth was impeded by abnormally dry years until 2011. After 2011, the increase in the vegetation cover continues in correspondence with increases in rainfall and soil moisture (Figures 3c and 3d and Table 2). In absolute numbers, the growing season FCover increases from 69% in 1999/2000 to 81% in 2017, and growing season NDVI increases from 0.73 to 0.79 over the same period. Note that NDVI values at that level are known to be in the range prone to saturation effects when compared to biomass volumes (Tian et al., 2016). The strong increase can be related to an average tree plantation area of 19 183 km^2 per year (Figure 3e), which is likely to have a great impact on the vegetation cover and accumulated biomass.

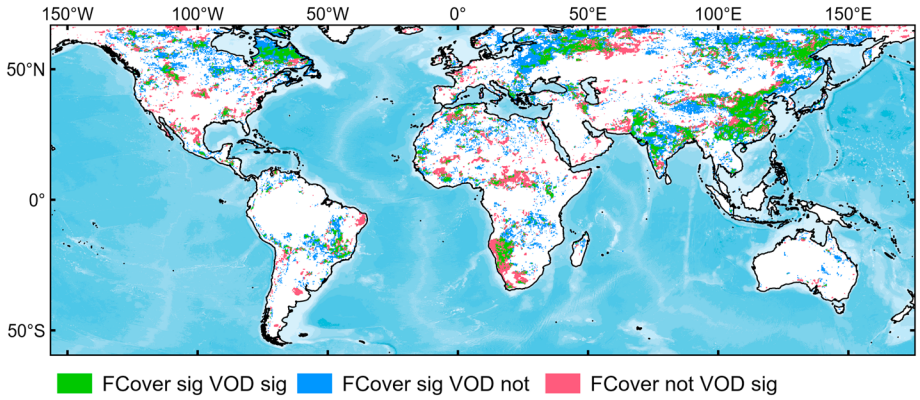

Figure 6. Spatial agreement of significant ($P < 0.05$) increase in vegetation cover (GEOV2 FCover) and biomass (X-VOD) for 1999–2012.

Indeed, tree planting activities, which reach their maximum number in 2015 (~31,000 km^2), primarily take place on sloping hills, and there is a clear and significant ($P < 0.01$) relationship between changes in vegetation cover and both terrain slopes and elevation, with a majority of the increases happening in ~2,500 m above sea level (Figures 5b and 5c). However, the spatial resolution of 1 km impedes a clearer picture and higher resolution analyses are required.

To better analyze the co-variations of biomass and vegetation cover, we estimate the global areas with significant positive trends ($P < 0.05$) both in growing season FCover and X-VOD for 1999–2012. We find that the Chinese karst area is among the largest spatially coherent area with increases in both vegetation cover and biomass for this period (Figure 6).

4. Discussion

All data sets applied in this study highlight South China Karst as a global hot spot of vegetation growth. We find that the area is globally one of the largest coherent regions with positive biomass and vegetation cover trends (1999–2017). This result underlines the region as being unique in relation to recent vegetation dynamics, and also in relation to the fact that other large hot spots of greening, like the Sahel (Hickler et al., 2005), the tropics (Nemani et al., 2003), or the northern ecosystems (Forkel et al., 2016), are mostly driven by climatic factors. In contrast, rainfall trends are negative in the earlier years (1999–2011) and the karst appears to have benefited from the effects of forestry practice and conservation management starting in 2001. This supports the results of Tong et al. (2018), which find positive vegetation trends in areas of high conservation efforts in the southern parts of the karst region. Only in the later years (2012–2017) favorable rainfall and soil moisture conditions have supported the vegetation growth. Moreover, other studies assessing global/regional greening primarily refer to vegetation primary productivity (Nemani et al., 2003; Zhang et al., 2017; Zhu et al., 2016). The karst region is among the globally largest regions where a significant increase in vegetation cover co-occurs with a significant increase in biomass.

Our study is limited to above-ground vegetation biomass, but an increase in soil carbon is likely to be linked with the observed biomass changes, as solid evidence that conservation opens for sequestering carbon in the soil exist (Liu et al., 2014). This increased biomass and carbon sequestration is not only important for the provisioning of ecological services in the karst area at local and regional scale (Ouyang et al., 2016) but also has likely impact on the global carbon budget. This shows that conservation, if applied at large scale, may offset or at least partly balance global carbon losses from deforestation and land cover transformation that happens in large parts of the world (Brandt et al., 2017). After several dry years around 2010 (Luo et al., 2016), rainfall and soil moisture conditions in southwest China were increasingly favorable during recent years (2012–2017) and the planted and protected woody vegetation certainly benefits from sufficient rainfall. However, the strongly positive trends of vegetation cover and biomass contrasting the negative trends in rainfall in the earlier years (1999–2010) suggest that tree plantings (on an average area of ~20,000 km^2 per year) and land cover conversion have strongly impacted the observed phenomenon (Cai et al., 2014; Xiao, 2014).

Our study supports that conservation projects have caused a positive regreening effect in southern China, helping to offset land degradation and contributing to climate change mitigation when studied at a large spatial extent (Tong et al., 2018). The substantial investments in ecological conservation and restoration in South China karst significantly improve the vegetation cover at large spatial scale, even under unfavorable weather condition. To ensure rapid growth of the plantations and to provide potential future timber profits to local livelihoods, some programs have, however, led to large scale planting of monocultures of nonnative trees on land that was formerly used for agriculture or that could potentially have been restored to native vegetation (Delang & Yuan, 2015). Such plantations may be highly vulnerable to disturbances other than drought (e.g., pest and diseases), are poor habitats for native species, and are thus potentially less ecologically resilient as compared to vegetation of higher biodiversity (Cao, 2011; Delang & Yuan, 2015). In addition, the extent of afforestation has potentially negative effects on regional food production by reducing areas of arable land with consequences related to local community resilience, regional food security, and export of the environmental cost of agriculture to other parts of the world (Delang & Yuan, 2015). On the other hand, farmers were able to improve their farming techniques supporting a general increase in food production during the Grain to Green Project phase (Cao, 2011; Cao et al., 2011). The increase in vegetation cover and biomass can be considered a success of global significance, but local ecological and economical problems remain and should not be overlooked (Cao et al., 2017; Cao, 2011; Chen et al., 2015). For further implementations of ecological conservation in South China Karst and elsewhere, the specific restoration measures should also consider the spatial and regional differences under various terrain and landform conditions.

Optical satellite sensors are able to reliably detect significant increases in the vegetation cover, but the biomass increase observed by L-VOD over 2011–2017 is higher than the increase in vegetation cover. This could be related to the fact that low-frequency microwave sensors are able to assess biomass accumulations below the canopy of densely vegetated areas. However, a quantification of L-VOD dynamics in biomass units could not yet be applied.

The data sets used here are state-of-the-art with unprecedented opportunities for exploring land surface dynamics, yet not free of uncertainties. GEOV2 FCover time series include a shift from the VGT-2 to the PROBA-V sensor in 2014. However, the data set has shown to be consistent with MODIS with the advantage of an additional year (1999) and providing biophysical variables at a high temporal frequency (10-day), continuity (gap-filled data), and smoothness (less affected by noise in the data). Also, the applied X-VOD time series is a combination of several sensors (Liu et al., 2015); the temporal consistency is found to be high (Tian et al., 2016). Finally, RFIs are a source of noise for SMOS based data over China (Oliva et al., 2012). The generated SMOS-IC data set is thoroughly filtered, but the impact of RFI needs to be further investigated as the data set is new. Taken together, the general trends of all data sets are consistent for the study area and there is a convergence of evidence that Southern China is a global hot spot of vegetation growth and biomass accumulation.

5. Conclusion

We have generated and used time series data sets derived from complementary state-of-the-art satellite systems to analyze a phenomenon of global significance: the greening of the South China Karst region. This greening is associated with a substantial increase in biomass, detected by EO systems for quantifying temporal changes in biomass that go beyond current capabilities of sensing vegetation changes primarily in the upper canopy layer. The application of VOD in the context of Chinese tree planting and conservation projects has shown the relevance of the data sets at regional and global scales, as well as its usefulness for biomass monitoring in the context of governmental initiatives and ecological assessments. Large parts of the observed biomass increase in Southern China can be considered as a direct or indirect effect of forestry and conservation efforts, supported by high annual rainfall and soil moisture in the later years providing the necessary conditions for the vegetation to grow. The increase in biomass is found to be of global significance, and future studies need to explore the effects of observed changes in terms of carbon stocks.

Acknowledgments
This study was funded by National Key Research and Development Program of China (2016YFC0502400), the Chinese Academy of Sciences President's International Fellowship Initiative (2018VCC0012), and the National Natural Science Foundation of China (41471445 and 41371418), as well as the Danish Council for Independent Research (DFF) grant ID: DFF-6111-00258. This research work was also funded by CNES (Centre National d'Etudes Spatiales) through the Science TOSCA (Terre Océan Surfaces Continentales et Atmosphère) program. A.V. acknowledges support from the EC Copernicus Global Land Service (CGLOPS-1 and 199494-JRC). We thank the European Space Agency (ESA) Support to Science Element (STSE) program and SMOS Expert Support Laboratory (ESL) for funding this study. We thank http://www.naturalearthdata.com for providing background maps and the OSGEO community for free software. All data sets are freely available: SMOS-IC L-VOD and soil moisture will be available at the Centre Aval de Traitement des Données SMOS (CATDS). X-VOD can be downloaded at http://www.wenfo.org/wald/global-biomass/. ESA CCI soil moisture can be found at http://www.esa-soilmoisture-cci.org/ and CHIRPS rainfall at http://chg.geog.ucsb.edu/data/chirps/. GEOV2 data are freely provided by the Copernicus Global Land Service (http://land.copernicus.eu/global/).

References

Brandt, M., Rasmussen, K., Peñuelas, J., Tian, F., Schurgers, G., Verger, A., et al. (2017). Human population growth offsets climate-driven increase in woody vegetation in sub-Saharan Africa. *Nature Ecology & Evolution*, *1*, 0081. https://doi.org/10.1038/s41559-017-0081

Brandt, M., Wigneron, J.-P., Chave, J., Tagesson, T., Penuelas, J., Ciais, P., et al. (2018). Satellite passive microwaves reveal recent climate-induced carbon losses in African drylands. *Nature Ecology & Evolution*, *2*(5), 827–835. https://doi.org/10.1038/s41559-018-0530-6

Cai, H., Yang, X., Wang, K., & Xiao, L. (2014). Is forest restoration in the southwest China karst promoted mainly by climate change or human-induced factors? *Remote Sensing*, *6*(10), 9895–9910. https://doi.org/10.3390/rs6109895

Cao, S. (2008). Why large-scale afforestation efforts in China have failed to solve the desertification problem. *Environmental Science & Technology*, *42*(6), 1826–1831.

Cao, S. (2011). Impact of China's large-scale ecological restoration program on the environment and society in arid and semiarid areas of China: Achievements, problems, synthesis, and applications. *Critical Reviews in Environmental Science and Technology*, *41*(4), 317–335. https://doi.org/10.1080/10643380902800034

Cao, S., Chen, L., Shankman, D., Wang, C., Wang, X., & Zhang, H. (2011). Excessive reliance on afforestation in China's arid and semi-arid regions: Lessons in ecological restoration. *Earth-Science Reviews*, *104*(4), 240–245. https://doi.org/10.1016/j.earscirev.2010.11.002

Cao, S., Ma, H., Yuan, W., & Wang, X. (2014). Interaction of ecological and social factors affects vegetation recovery in China. *Biological Conservation*, *180*, 270–277. https://doi.org/10.1016/j.biocon.2014.10.009

Cao, S., Shang, D., Yue, H., & Ma, H. (2017). A win-win strategy for ecological restoration and biodiversity conservation in Southern China. *Environmental Research Letters*, *12*(4), 044004. https://doi.org/10.1088/1748-9326/aa650c

Cao, S., & Zhang, J. (2015). Political risks arising from the impacts of large-scale afforestation on water resources of the Tibetan Plateau. *Gondwana Research*, *28*(2), 898–903. https://doi.org/10.1016/j.gr.2014.07.002

Cao, S., Zhang, J., Chen, L., & Zhao, T. (2016). Ecosystem water imbalances created during ecological restoration by afforestation in China, and lessons for other developing countries. *Journal of Environmental Management*, *183*, 843–849. https://doi.org/10.1016/j.jenvman.2016.07.096

Chen, B., Jin, D., Ma, J., Zhou, X.-L., Huang, Y., & Yan, Y.-H. (2015). High risk of plant invasion in the understory of eucalypt plantations in South China. *Scientific Reports*, *5*, 18492. https://doi.org/10.1038/srep18492

Delang, C. O., & Yuan, Z. (2015). *China's grain for green program*. Cham: Springer International. https://doi.org/10.1007/978-3-319-11505-4

Du, J., Kimball, J. S., Jones, L. A., Kim, Y., Glassy, J., & Watts, J. D. (2017). A global satellite environmental data record derived from AMSR-E and AMSR2 microwave Earth observations. *Earth System Science Data*, *9*(2), 791–808. https://doi.org/10.5194/essd-9-791-2017

Enenkel, M., Reimer, C., Dorigo, W., Wagner, W., Pfeil, I., Parinussa, R., & De Jeu, R. (2016). Combining satellite observations to develop a global soil moisture product for near-real-time applications. *Hydrology and Earth System Sciences*, *20*(10), 4191–4208. https://doi.org/10.5194/hess-20-4191-2016

Fang, J., Guo, Z., Hu, H., Kato, T., Muraoka, H., & Son, Y. (2014). Forest biomass carbon sinks in East Asia, with special reference to the relative contributions of forest expansion and forest growth. *Global Change Biology*, *20*(6), 2019–2030. https://doi.org/10.1111/gcb.12512

Fensholt, R., Langanke, T., Rasmussen, K., Reenberg, A., Prince, S. D., Tucker, C., et al. (2012). Greenness in semi-arid areas across the globe 1981–2007—An Earth Observing Satellite based analysis of trends and drivers. *Remote Sensing of Environment*, *121*, 144–158. https://doi.org/10.1016/j.rse.2012.01.017

Fernandez-Moran, R., Al-Yaari, A., Mialon, A., Mahmoodi, A., Al Bitar, A., De Lannoy, G., et al. (2017). SMOS-IC: An alternative SMOS soil moisture and vegetation optical depth product. *Remote Sensing*, *9*(5), 457. https://doi.org/10.3390/rs9050457

Forkel, M., Carvalhais, N., Rödenbeck, C., Keeling, R., Heimann, M., Thonicke, K., et al. (2016). Enhanced seasonal CO2 exchange caused by amplified plant productivity in northern ecosystems. *Science*. https://doi.org/10.1126/science.aac4971

Funk, C., Peterson, P., Landsfeld, M., Pedreros, D., Verdin, J., Shukla, S., et al. (2015). The climate hazards infrared precipitation with stations—A new environmental record for monitoring extremes. *Scientific Data*, *2*, 150066. https://doi.org/10.1038/sdata.2015.66

Guglielmetti, M., Schwank, M., Mätzler, C., Oberdörster, C., Vanderborght, J., & Flühler, H. (2007). Measured microwave radiative transfer properties of a deciduous forest canopy. *Remote Sensing of Environment*, *109*(4), 523–532. https://doi.org/10.1016/j.rse.2007.02.003

Hickler, T., Eklundh, L., Seaquist, J. W., Smith, B., Ardö, J., Olsson, L., et al. (2005). Precipitation controls Sahel greening trend. *Geophysical Research Letters*, *32*, L21415. https://doi.org/10.1029/2005GL024370

Hua, F., Wang, X., Zheng, X., Fisher, B., Wang, L., Zhu, J., et al. (2016). Opportunities for biodiversity gains under the world's largest reforestation programme. *Nature Communications*, *7*, 12717. https://doi.org/10.1038/ncomms12717

Jiang, Z., Lian, Y., & Qin, X. (2014). Rocky desertification in southwest China: Impacts, causes, and restoration. *Earth-Science Reviews*, *132*, 1–12. https://doi.org/10.1016/j.earscirev.2014.01.005

Kerr, Y. H., Al-Yaari, A., Rodriguez-Fernandez, N., Parrens, M., Molero, B., Leroux, D., et al. (2016). Overview of SMOS performance in terms of global soil moisture monitoring after six years in operation. *Remote Sensing of Environment*, *180*, 40–63.

Konings, A. G., Piles, M., Das, N., & Entekhabi, D. (2017). L-band vegetation optical depth and effective scattering albedo estimation from SMAP. *Remote Sensing of Environment*, *198*, 460–470. https://doi.org/10.1016/j.rse.2017.06.037

Latifi, H., Fassnacht, F. E., Hartig, F., Berger, C., Hernández, J., Corvalán, P., & Koch, B. (2015). Stratified aboveground forest biomass estimation by remote sensing data. *International Journal of Applied Earth Observation and Geoinformation*, *38*(Supplement C), 229–241. https://doi.org/10.1016/j.jag.2015.01.016

Liu, D., Chen, Y., Cai, W., Dong, W., Xiao, J., Chen, J., et al. (2014). The contribution of China's Grain to Green Program to carbon sequestration. *Landscape Ecology*, *29*(10), 1675–1688. https://doi.org/10.1007/s10980-014-0081-4

Liu, Y. Y., van Dijk, A. I. J. M., de Jeu, R. A. M., Canadell, J. G., McCabe, M. F., Evans, J. P., & Wang, G. (2015). Recent reversal in loss of global terrestrial biomass. *Nature Climate Change*, *5*(5), 470–474. https://doi.org/10.1038/nclimate2581

Luo, H., Zhou, T., Wu, H., Zhao, X., Wang, Q., Gao, S., & Li, Z. (2016). Contrasting responses of planted and natural forests to drought intensity in Yunnan, China. *Remote Sensing*, *8*(8), 635. https://doi.org/10.3390/rs8080635

Momen, M., Wood, J. D., Novick, K. A., Pangle, R., Pockman, W. T., McDowell, N. G., & Konings, A. G. (2017). Interacting effects of leaf water potential and biomass on vegetation optical depth. *Journal of Geophysical Research: Biogeosciences*, *122*, 3031–3046. https://doi.org/10.1002/2017JG004145

Moore, J. C., Chen, Y., Cui, X., Yuan, W., Dong, W., Gao, Y., & Shi, P. (2016). Will China be the first to initiate climate engineering? *Earth's Future*, *4*, 588–595. https://doi.org/10.1002/2016EF000402

Myneni, R. B., & Hall, F. G. (1995). The interpretation of spectral vegetation indexes. *IEEE Transactions on Geoscience and Remote Sensing*, *33*(2), 481–486. https://doi.org/10.1109/36.377948

Nemani, R. R., Keeling, C. D., Hashimoto, H., Jolly, W. M., Piper, S. C., Tucker, C. J., et al. (2003). Climate-driven increases in global terrestrial net primary production from 1982 to 1999. *Science*, *300*(5625), 1560–1563. https://doi.org/10.1126/science.1082750

Oliva, R., Daganzo, E., Kerr, Y. H., Mecklenburg, S., Nieto, S., Richaume, P., & Gruhier, C. (2012). SMOS radio frequency interference scenario: Status and actions taken to improve the RFI environment in the 1400 #x2013;1427-MHz passive band. *IEEE Transactions on Geoscience and Remote Sensing*, *50*(5), 1427–1439. https://doi.org/10.1109/TGRS.2012.2182775

Ouyang, Z., Zheng, H., Xiao, Y., Polasky, S., Liu, J., Xu, W., et al. (2016). Improvements in ecosystem services from investments in natural capital. *Science*, *352*(6292), 1455–1459. https://doi.org/10.1126/science.aaf2295

Piao, S., Yin, G., Tan, J., Cheng, L., Huang, M., Li, Y., et al. (2015). Detection and attribution of vegetation greening trend in China over the last 30 years. *Global Change Biology*, *21*(4), 1601–1609. https://doi.org/10.1111/gcb.12795

Rodríguez-Fernández, N. J., Mialon, A., Mermoz, S., Bouvet, A., Richaume, P., Al Bitar, A., et al. (2018). The high sensitivity of SMOS L-Band vegetation optical depth to biomass. *Biogeosciences Discussions*, *2018*, 1–20. https://doi.org/10.5194/bg-2018-49

Tian, F., Brandt, M., Liu, Y. Y., Verger, A., Tagesson, T., Diouf, A. A., et al. (2016). Remote sensing of vegetation dynamics in drylands: Evaluating vegetation optical depth (VOD) using AVHRR NDVI and in situ green biomass data over West African Sahel. *Remote Sensing of Environment*, *177*, 265–276. https://doi.org/10.1016/j.rse.2016.02.056

Tian, F., Fensholt, R., Verbesselt, J., Grogan, K., Horion, S., & Wang, Y. (2015). Evaluating temporal consistency of long-term global NDVI datasets for trend analysis. *Remote Sensing of Environment*, *163*, 326–340. https://doi.org/10.1016/j.rse.2015.03.031

Tong, X., Brandt, M., Yue, Y., Horion, S., Wang, K., Keersmaecker, W. D., et al. (2018). Increased vegetation growth and carbon stock in China karst via ecological engineering. *Nature Sustainability*, *1*(1), 44–50. https://doi.org/10.1038/s41893-017-0004-x

Tong, X., Wang, K., Yue, Y., Brandt, M., Liu, B., Zhang, C., et al. (2017). Quantifying the effectiveness of ecological restoration projects on long-term vegetation dynamics in the karst regions of southwest China. *International Journal of Applied Earth Observation and Geoinformation*, *54*, 105–113. https://doi.org/10.1016/j.jag.2016.09.013

Tucker, C. J. (1979). Red and photographic infrared linear combinations for monitoring vegetation. *Remote Sensing of Environment*, *8*(2), 127–150. https://doi.org/10.1016/0034-4257(79)90013-0

Verger, A., Baret, F., & Weiss, M. (2014). Near real-time vegetation monitoring at global scale. *IEEE Journal of Selected Topics in Applied Earth Observations and Remote Sensing*, *7*(8), 3473–3481. https://doi.org/10.1109/JSTARS.2014.2328632

Vittucci, C., Ferrazzoli, P., Kerr, Y., Richaume, P., Guerriero, L., Rahmoune, R., & Laurin, G. V. (2016). SMOS retrieval over forests: Exploitation of optical depth and tests of soil moisture estimates. *Remote Sensing of Environment*, *180*, 115–127. https://doi.org/10.1016/j.rse.2016.03.004

Wigneron, J.-P., Chanzy, A., Calvet, J.-C., & Bruguier, N. (1995). A simple algorithm to retrieve soil moisture and vegetation biomass using passive microwave measurements over crop fields. *Remote Sensing of Environment*, *51*(3), 331–341. https://doi.org/10.1016/0034-4257(94)00081-W

Wigneron, J.-P., Jackson, T. J., O'Neill, P., De Lannoy, G., de Rosnay, P., Walker, J. P., et al. (2017). Modeling the passive microwave signature from land surfaces: A review of recent results and application to the L-band SMOS & SMAP soil moisture retrieval algorithms. *Remote Sensing of Environment*, *192*, 238–262. https://doi.org/10.1016/j.rse.2017.01.024

Wigneron, J.-P., Kerr, Y., Waldteufel, P., Saleh, K., Escorihuela, M.-J., Richaume, P., et al. (2007). L-band microwave emission of the biosphere (L-MEB) model: Description and calibration against experimental data sets over crop fields. *Remote Sensing of Environment*, *107*(4), 639–655. https://doi.org/10.1016/j.rse.2006.10.014

Xiao, J. (2014). Satellite evidence for significant biophysical consequences of the "Grain for Green" Program on the Loess Plateau in China. *Journal of Geophysical Research: Biogeosciences*, *119*, 2261–2275. https://doi.org/10.1002/2014JG002820

Zhang, C., Qi, X., Wang, K., Zhang, M., & Yue, Y. (2017). The application of geospatial techniques in monitoring karst vegetation recovery in southwest China: A review. *Progress in Physical Geography*, *41*(4), 450–477. https://doi.org/10.1177/0309133317714246

Zhang, J., Dai, M., Wang, L., & Su, W. (2016). Household livelihood change under the rocky desertification control project in karst areas, southwest China. *Land Use Policy*, *56*(Supplement C), 8–15. https://doi.org/10.1016/j.landusepol.2016.04.009

Zhang, N., Shi, J., Sun, G., Guo, Z., & Chai, L. (2011). Assessment of boreal forest biomass using L-band radiometer SMOS data. In *2011 IEEE International Geoscience and Remote Sensing Symposium* (pp. 1946–1949). Vancouver: IEEE Xplore. https://doi.org/10.1109/IGARSS.2011.6049507

Zhang, Y., Peng, C., Li, W., Tian, L., Zhu, Q., Chen, H., et al. (2016). Multiple afforestation programs accelerate the greenness in the 'Three North' region of China from 1982 to 2013. *Ecological Indicators*, *61*, 404–412. https://doi.org/10.1016/j.ecolind.2015.09.041

Zhu, Z., Piao, S., Myneni, R. B., Huang, M., Zeng, Z., Canadell, J. G., et al. (2016). Greening of the Earth and its drivers. *Nature Climate Change*, *6*(8), 791–795. https://doi.org/10.1038/nclimate3004